Transverse reinforcement optimization of a precast special roof element through an experimental and numerical procedure

Transverse reinforcement optimization of a precast special roof element through an experimental and numerical procedure

Patrizia Bernardi [a], Roberto Cerioni [a], Elena Michelini [a], Alice Sirico[a] *

[a] Department of Engineering and Architecture, University of Parma,

Parco Area delle Scienze 181/A, 43124 Parma - Italy

* Corresponding author. Tel. +39 0521 905709; fax +39 0521 905924

E-mail address: alice.sirico@unipr.it (A. Sirico).

ABSTRACT

The transverse behavior of a long span three-plate precast roof element is investigated by means of an experimental and numerical research. The performed study highlights that the failure mode of this folded-plate element is strongly influenced by the amount of transverse reinforcement in the wings. This latter is usually designed through simplified methods, which often lead to over-dimensioning in terms of steel welded mesh. To avoid excessive costs for the producers, transverse reinforcement optimization should be required. In this work, a non-linear FE modelling was applied for this purpose. The reliability of the followed numerical procedure was first verified by an initial type testing (i.e. experimental load test up to failure). The agreement between numerical and experimental results showed the efficiency of the model in simulating all the main sources of non-linearity related to both material behavior and element geometry. Numerical analyses were so used to perform a parametric study as a function of transverse reinforcement amount, aimed at determining a coefficient of "model inaccuracy". This coefficient should be used as a correction factor for the element design in routine calculations based on beam theory.

Keywords: *precast special roof element; full-scale test; thin-walled open cross section; mechanical non-linearity; geometric non-linearity; Finite Element modelling; transverse reinforcement design.*

1 Introduction

Thin-walled elements made of steel, reinforced concrete, composite or hybrid materials are quite widespread in modern structures, owing to the increasing need of saving material and weight. However, due to the small thickness of their cross sections profile, these elements are sensitive to problems that arise from large deflections, structural instabilities and vibrations, and consequently their behavior has been object of several studies [1–5].

Thin-walled structural elements with deformable transverse profile, such as folded-plate or shell elements, are also adopted in the realization of roofing systems, and they are usually referred to as "special roof elements" according to European Standard EN 13693:2009 [6]. This type of elements combines the overall flexural behavior along the main span with a complex distribution of in-plane forces and local moments.

One of the main issues related to the use of precast roof elements is represented by their correct design with respect to transverse bending. In general, the presence of transverse stresses in the cross section is due to the loads transmitted by complementary elements (i.e. reinforced concrete or metal slabs, with plane or curved shape), which in turn depend on their dead weight and spacing. The cross section shape plays a major role in transverse stress distribution, too. Stress concentration takes usually place in the element wings and can determine an early transverse failure with respect to longitudinal one.

The most common technical solutions adopted by manufacturers so as to avoid a brittle wing failure can be different. A first solution, often used in case of open core roof elements, consists in increasing the concrete thickness in the bottom part of the wings and/or increasing the transverse reinforcement, which is generally constituted by welded wire meshes. Alternatively, wings can be connected to each other through suitable elements, which can be discrete or continuous. In the first case, transverse connection between wings is made through the insertion of properly spaced steel ties, while in the second one wings are connected by means of a thin concrete slab with a stiffening function, so realizing a closed-core section. The design of both wing reinforcement and steel ties, if

present, is usually carried out with reference to simplified methods (e.g. fixed-end bending moments of cantilever wings), which are used as an integration of the main longitudinal calculations, according to EN 13693:2009 [6] and Eurocode 2 [7]. These approaches do not consider the effects of geometric and mechanical non-linearity, which can instead significantly influence the element structural behavior and especially its collapse, as proved by the limited experimental tests and by the numerical studies available in technical literature (e.g. [8–12]).

In case of folded-plate systems (made of three or more non convergent plates), like the one considered in this work, EN 13693:2009 [6] suggests to perform more complex numerical analyses, inclusive of transverse flexural effects due to loads and to the deformation of the cross section profile. For units with constant cross section, the Finite Strip Method can be applied [13,14]; otherwise the Finite Element (FE) method can be generally used. Anyway, in case of regular shapes the abovementioned European Standard allows to adopt a beam-like routine calculation for the main longitudinal behavior, adjusted with the results of initial type calculations made with more accurate analytical models. Transverse flexural effects can be given by models derived from the same initial type calculations, properly verified by initial type testing (that is to say load tests up to failure).

In this work, an attempt was made to provide an estimate of the influence of transverse behavior on the bearing capacity of a long span special roof element. The study was carried out through subsequent phases, as usually done for other precast structures with non-standard geometry (e.g. [15]). An experimental test was first carried out on a full-scale specimen and the obtained results were used to prove the effectiveness of a non-linear numerical procedure based on the FE method. This procedure was then applied to a parametric study for the optimization of transverse reinforcement. The goal was to find a proper amount of transverse reinforcement such as to prevent an early transverse failure and at the same time to avoid an unnecessary use of steel. The obtained numerical results were properly summarized so to obtain one single parameter including all sources of non-linearity, which can be used for a quick, safe and economical design of these elements.

2 Experimental test

The experimental test was carried out on a three-plate thin-walled element belonging to an Italian manufacturer company. This precast element is used for the realization of roofing systems in industrial buildings (Fig.1a) and can reach a maximum length of 30 m. Complementary elements constituted by metal or Reinforced Concrete (RC) barrel-vault shell, or shed shell with skylights are generally adopted. Typical interaxis spacing values range from 4.5 to 5.5 m.

2.1 Roof element description and material properties

The investigated specimen was characterized by an open cross section formed by three plates: two 41 - degrees inclined wings with variable thickness, ranging from about 52 to 155 mm, and a bottom chord with a constant thickness of 125 mm (Fig. 1b). The slenderness ratio of the tested element was chosen to be representative of current production, resulting in a depth of 0.9 m and a length of 24 m. The specimen was reinforced with 25 prestressing strands placed in the bottom chord and having a diameter of 1/2" (93 mm). Near the supports, 8 strands were coated: six of them for a length of 1 m and the other two for 2 m. Details of reinforcement arrangement, including ordinary steel bars, stirrups and welded meshes are given in Figure 1b for the current cross section, starting at 1.5 m from element heads. The transverse reinforcement arrangement was designed for the test with reference to a severe loading condition corresponding to 5.5 m spacing between the roof elements, with interposed ribbed concrete slabs. The welded meshes were thickened near the heads of the element, where also 6Φ10 mm and 2Φ20 mm steel forks were added.

Normal-strength concrete of class C45/55 with maximum aggregate size of 12 mm was used for specimen casting. The mean value of concrete compressive strength at the day of testing was determined on cubes extracted from the same batch and subjected to the same curing conditions of the investigated roof element. B450C steel grade was adopted for ordinary reinforcement, while prestressing steel with a characteristic tensile strength f_{pk} of 1860 MPa was used for strands. Mean values of ordinary and prestressing steel strength were deduced from the corresponding tensile tests

carried out by the producers for steel certification. Table 1 summarizes the mean values of concrete and steel mechanical properties.

2.2 Test setup and procedure

The full-scale flexural test on the above described precast roof element was performed at the production plant of the manufacturer company (Fig. 2), in compliance with the Product Standard for special roof elements EN 13693:2009 [6]. The element was simply supported over a net span of 23.50 m (see Figures 2b,c for the adopted support arrangement). The design load distribution was simulated by means of concentrated forces applied in three sections over the span, placed at midspan as well as at one-sixth of the span (Fig. 3a). This is in accordance with the guidelines for flexural tests of elements provided by the Product Standard [6] to simulate uniform design load distribution through concentrated test forces. More in detail, in each of these loading sections a central load (named P_c in Figure 3) was applied on the bottom chord. To guarantee a better load distribution, a properly designed system of U channel and I steel beams was provided (Figs. 3b,c). Furthermore, two point loads (named P_w in Figure 3) were applied on the top of each wing and distributed through 2 m long I beams (Figs. 3b,c), so to represent the reaction forces transmitted by complementary elements. All the loads were applied by means of hydraulic jacks and increased until failure according to the sequence reported in Table 2. Three loading cycles were performed: the two first preliminary loading-unloading cycles were designed so as to reach the total load corresponding to the SLS condition for the element, while in the third cycle the load was increased until failure.

During the test, vertical and horizontal displacements were recorded by transducers placed at supports, at midspan and at one-sixth of the span (denoted as D and W in Figures 4a,b, see also Figures 5b,c). Furthermore, strain gauges were placed in the two cross sections at one-third of the span, to get longitudinal and transverse strains (Figs. 4a,c,d; Fig. 5a). It is worth noticing that all the instruments, except for the transducers for the measurements of vertical displacement at midspan, were removed before the attainment of failure.

2.3 Main experimental results

Some experimental results were reported in terms of total load P vs. vertical displacement of the bottom chord (δ_c) at midspan and in the two sections at one-sixth of the span (Fig.6a), and in terms of total load P vs. transverse strain (ε_t) at the intrados of the bottom chord and at the extrados of the wings (Fig.6b). These latter strains were measured with two strain gauges placed at about mid-height of the wing. The same graphs also report the total design load acting on the investigated element at SLS, ULS and that corresponding to the attainment of the ultimate longitudinal sectional moment resistance, evaluated according to [7] considering both design (M_{Rd}) and mean experimental material strengths (M_{Rmean}). From the exam of Figure 6a, it can be observed that the experimental failure load (P_{test}) of the thin-walled element was lower than the load (P_{calc}) corresponding to M_{Rmean}, with a ratio $\eta_0 = P_{test} / P_{calc} = 0.78$. This is because the ultimate condition of this kind of long span roof elements with open cross section is often reached for a combination of longitudinal and transverse stresses, together with second order effects. These effects are in turn related to the loss of shape of the cross section in its own plane and, like in the examined case, they can cause an earlier transverse failure than that due to longitudinal bending. A crucial parameter ruling the failure mode is the amount of transverse reinforcement, which was designed intentionally to produce a transverse failure of the tested specimen. One of the main goals of the experimental test was indeed to verify the effectiveness of the adopted numerical procedure in reproducing the failure mode also when it is governed by second order effects. The final aim was then to adopt the procedure for the optimization of transverse reinforcement, so to avoid an early failure of the element while reducing at the same time the amount of stirrups with their related costs.

The evolution of the experimental crack pattern, which is representative of the response of the element to the imposed loads, also confirmed the above described failure mode. After the reaching of SLS loading, almost vertical flexural cracks developed at midspan (Fig. 7a). As loading increased, these cracks became deeper and spread towards supports, resulting in inclined flexure-shear (Fig. 7b) and

diagonal shear cracks (Figs. 7c,d). Failure was accompanied by the loss of shape of the cross section (Fig.7f), which caused the development of longitudinal cracks at mid-height of the wings (Fig. 7e).

3 Finite Element modelling

The behavior of the above described thin-walled precast roof element was numerically studied by means of FE analyses, carried out with the commercial software ABAQUS [16], and accounting for both geometric and mechanical non-linearity. Geometric non-linearity was considered by simply setting the "NLGEOM" option in the adopted FE code, so to follow the large deformation theory. Material non-linearity was accounted by implementing the 2D-PARC constitutive model [17,18] into the FE procedure. This model, which belongs to fixed smeared crack formulations, allows to take into account several non-linear mechanisms that influence Reinforced Concrete (RC) behavior, such as concrete cracking and crushing, aggregate bridging and interlock, bond-slip behavior, dowel action and yielding of the reinforcement. The main features of the model are briefly recalled in Section 3.1.

3.1 Constitutive model for reinforced concrete

2D-PARC model is written in the form of a total-load secant stiffness matrix into a User Defined Material Subroutine (UMAT) to be recalled by ABAQUS, for each integration point of each element both before and after cracking.

In the uncracked stage, the total stiffness matrix is obtained by summing up concrete and steel contribution, since perfect bond is assumed between them. An elastic-hardening behavior is considered for steel. A non-linear elastic formulation is followed for concrete, accounting for material non-linearity both under uniaxial and biaxial state of stress[17,18].

When the current state of stress violates the concrete failure envelope in the compressive region, concrete crushing appears [18]; while when the failure limit is reached in the tensile region, the transition to the cracked stage takes place for the considered integration point. Cracking is assumed

to develop perpendicular to the direction of the maximum principal stress corresponding to crack initiation and its orientation remains fixed as loading increases.

A strain decomposition procedure is adopted in the cracked stage: the total strain is subdivided into two components, respectively related to the whole, even though damaged, RC between cracks and to all the resistant mechanisms that develop at crack surfaces. Each mechanical phenomenon is individually analyzed by considering local stresses and strains at crack location and then the corresponding contribution is inserted into the crack stiffness matrix, on the basis of proper laws available in technical literature. The details concerning the constitutive relations adopted for the modelling of each contribution can be found in [17].

The behavior of RC between cracks is described by adopting the same approach used in the uncracked stage, even if a slight modification is operated on both concrete and steel stiffness matrices, so as to account for the degradation induced by cracking.

For each integration point and iteration within the loading increment, 2D-PARC computes the total stiffness matrix and the updated total stresses. They are then passed to ABAQUS, which performs all the subsequent operations required to solve the problem.

3.2 Modelling choices

4-node shell elements with one Gauss integration point in the plane and three Simpson integration points in the thickness (denoted as "S4R" in ABAQUS) were used to model the thin-walled roof element described in Section 1. A further refinement by using a higher number of integration points in the thickness of the shell element was tried, but the rate of improvement of numerical results was not comparable with the greater computational effort required.

While conventional reinforcement was smeared within each element according to 2D-PARC model hypotheses, prestressing strands were embedded into the FE mesh through the ABAQUS's "REBAR LAYER" option. Prestressing was assigned by imposing a not equilibrated initial condition in the first step of the numerical analysis in order to obtain the actual state of stress of both concrete and

strands before the application of external loads. The final prestressing to be assigned was estimated by considering both immediate and time dependent stress losses, according to Eurocode 2 [7]. The transfer of prestressing was simulated by adopting a linear function over the transmission length, once again evaluated according to [7]. A mesh refinement was adopted within the transmission length in order to gradually apply prestressing stress variations.

Strand mechanical behavior was modelled through an elastic-hardening stress-strain relationship calibrated on the basis of the experimental strengths, recalled in Table 1. In the same Table also the mechanical properties of concrete and ordinary reinforcement adopted in the analysis were reported.

In order to reduce computational efforts, only half of the transverse cross section was modelled because of the symmetry of both geometry and loading conditions. Even if the element – and particularly wing – behavior could be affected by the presence of imperfections, their influence was neglected due to the complexity of the modelling. However, in the light of the findings reported in Section 3.3, local instability problems, triggered by imperfections, did not occur during the test.

Test loads on the wings and on the bottom chord were simulated with nodal forces within the experimental loading footprint area. The following loading sequence was adopted: 1) prestressing, 2) element dead load, 3) loads of the third loading cycle of the experimental test, according to Table 2.

Special attention was paid to the modelling of support conditions. During the experimental test, the supports undergone a not negligible vertical displacement. In order to correctly represent this constraint condition, spring elements were inserted into the model. The evolution of their stiffness as loading increases was calibrated on the basis of the experimental measurement of vertical displacement at supports (see Fig. 8). For comparisons, in Section 3.3 experimental evidences were also compared to numerical results obtained by assuming fixed supports.

3.3 Comparison between numerical and experimental results

Results obtained from the numerical model were compared to the experimental ones in terms of displacements, strains and crack pattern evolution. These comparisons highlight that the numerical

model was able to reproduce the actual response of the element during the test, and in particular its failure mode, related to transverse flexure and second order effects. It is worth noticing that, according to the hypotheses of the adopted model, failure is assumed to happen in correspondence of the attainment of the first of the following conditions: achievement of 0.1% proof stress in prestressing strands or of a conventional limit strain in welded meshes, ordinary steel bars or stirrups. In the performed analysis, longitudinal stresses recorded in the strands were far from the assumed limit value, being their maximum value in correspondence of numerical failure equal to about 1340 MPa. On the contrary, numerical failure was characterized by high values of transverse strains in the welded mesh, and, at the same time, by large values of crack opening in the wings.

Comparisons between numerical and experimental results in terms of total load P vs. vertical displacement of the bottom chord (δ_c) and of the wings (δ_w), at midspan (L/2) and at one-sixth of the span (L/6), were shown in Figures 9a-d. Element dead load, which was included in the numerical analyses but acted before the beginning of the experimental test, was added to the total applied load in all the reported graphs. As already mentioned, the analyses were repeated twice, by considering either fixed or flexible supports with variable stiffness (referred to as "springs" in Figures 9-11). As can be seen, this last modelling allowed a better fitting of the experimental data, especially for loads greater than ULS ones. Numerical failure was almost equal to the experimental one, since the obtained ratio P_{test} / P_{NLFEA} was approximately equal to 1.01.

Figures 10a,b report the wing opening as a function of the total load in the two cross sections at L/6 and at supports, respectively. It can be noticed that in this case, the assumed support scheme does not influence numerical results, since the horizontal displacement predictions obtained with fixed and with flexible supports are almost coincident.

The model was able to catch the experimental behavior not only in terms of stiffness, load-deformation response and type of failure, but also in terms of strain, as shown in the graphs of Figure 11. For sake of clarity, only the results of the numerical analysis with variable stiffness supports were reported, being almost coincident with those obtained by assuming fixed supports. A satisfactory

agreement between numerical and experimental strain was registered for low loads, while results showed a greater scatter for higher values, when crack formation took place. The possible appearance of a crack in the gauge length during the experimental test or in the considered integration point during FE simulation makes indeed the strain values meaningless after cracking development. Moreover, it has to be observed that the onset of cracking is strongly dependent on the concrete tensile strength value inserted as input in the numerical model. In the performed analyses, this value was determined from experimental cube compressive strength through the relation suggested by Eurocode 2 [7], but in thin-walled sections concrete could exhibit a tensile strength different from conventional one, as also discussed in [19].

Further comparisons between numerical and experimental results were provided in terms of cracking development and crack width at failure, as depicted in Figures 12 and 13. It should be noticed that the reported numerical crack pattern is referred to the numerical failure load, which was very close to the experimental one, as observed from previous comparisons. The numerical model was able to correctly represent both the central flexural cracks, which developed from midspan towards supports during the test (Fig. 12a), and the longitudinal cracks which appeared at mid-height of the wings, both at intrados and at extrados (Fig. 12b and Fig.13), causing the failure of the element.

4 Design optimization of transverse reinforcement

The good agreement between experimental and numerical results allowed extending the proposed procedure to a numerical parametric study, so to further explore the influence of transverse reinforcement on failure mode.

NLFE analyses were carried out by considering in all the simulations the same cross section geometry, element span and material strength classes, which were set equal to those of the experimental specimen. Due to the design purpose of the parametric investigation, material design strength values were adopted instead of mean ones both for numerical analyses and for the evaluation of flexural resistance. Common design loads referred to different spacings between the thin-walled

roof elements and different types of complementary panels (heavy/light) were considered. It has to be noted that the presence of these complementary shells was introduced in the numerical model only through the transmitted vertical load, while any other effect on stress distribution induced by their interaction with the roof element (such as a possible arch effect) was neglected. More in details, two spacings between elements, respectively equal to 4.5 and 5.5 m, were considered, as well as two different types of complementary element between them, i.e. ribbed concrete slabs (representing the more severe and "heavy" loading condition), and curved metal panels (representing the "light" loading condition). Therefore, four reference design cases were identified, and they were named according to the designation reported in Table 3. In the same Table also the number of prestressing strands considered for each design case, due to the different imposed loads, as well as the corresponding design moment resistance M_{Rd}, computed by applying the classic beam theory were summarized. For each case reported in Table 3, the transverse reinforcement amount was optimized by modifying the diameter Φ or the spacing s of welded meshes n°2 and n°3 of Figure 1. Six different transverse reinforcement amounts (Φ6/200, Φ8/200, Φ8/150, Φ8/120, Φ8/100 and Φ10/120 mm) were then considered for each of the four cases, for a total of 24 analyses.

In FE simulations, loads were applied so as to simulate the usual distribution for the roof element: its cross section was uniformly loaded at the extrados, while at the top of the wings the reaction force transmitted by adjacent complementary elements was considered. The uniformly distributed load acting at element extrados was kept the same for all the investigated cases and accounted for the dead load of the thin-walled element, the permanent load (assumed equal to 0.15 kN/m^2 and corresponding to a waterproofing membrane), and the variable load due to snow (assumed equal to 1.2 kN/m^2). The loads at the top of the wings – namely due to complementary element dead load (i.e. 1.30 kN/m^2 and 0.15 kN/m^2 for the heavy and light solution, respectively), and to the same abovementioned permanent and variable loads – were calculated for each design case based on the complementary element extension. NLFE analyses were performed through different loading steps, namely: 1) prestressing, 2) roof element dead load, 3) external loads (uniformly distributed over the cross section

and concentrated at the top of the wings) until the attainment of SLS condition, 4) increase of external loads to reach ULS condition, 5) proportional increase of previously applied loads until roof element failure.

NLFE results were summarized in a "optimization design chart" (Fig. 14a) allowing the evaluation of the safety level related to the use of different percentages of transverse reinforcement. To this end, the coefficient of "model inaccuracy" η_0, previously expressed in Section 3.3 as the ratio P_{test} / P_{calc} according to EN 13693:2009, was redefined in terms of bending moment, as the ratio between the numerical failure moment M_{NLFEA} (as obtained from numerical analyses with material design strengths), and the longitudinal design sectional moment resistance M_{Rd} (see Table 3). So, since the proved agreement between NLFEA and test results, the coefficient η_0 can be seen as an index of the difference between the theoretical element strength and its effective structural response. This latter is influenced by several factors that are taken into account in NLFE analyses, such as geometric non-linearity – mainly depending on the effective cross-section shape and on the ratio between the load on the wings and on the bottom chord – and non-linear material behavior. It includes concrete cracking and crushing, stress redistribution between cracked and uncracked sections, as well as all the fundamental resistant mechanisms developing after cracking (such as aggregate interlock and bridging, tension stiffening and dowel action).

In the chart of Figure 14a this coefficient η_0 was reported as function of the amount of transverse reinforcement ρ. This latter was computed with reference to the area of welded mesh n°2, related to its spacing and to the minimum thickness of the wing (i.e. 52 mm). When $\eta_0 < 1$, a design procedure according to beam theory should be considered unsafe, since failure was strongly ruled by second order effects. For this reason, the design moment resistance M_{Rd} should be reduced by multiplying it for η_0. When $\eta_0 \geq 1$, a classic design according to beam theory might be in any case safe, since the actual structural response and so the bearing capacity of the element is improved by the abovementioned stress redistribution and resistant mechanisms developing after cracking. Failure

could be either for transverse or longitudinal flexure depending on the amount of transverse reinforcement. This fact was proved by repeating the same analyses, but with an increasing amount of transverse reinforcement. It can be observed that until transverse reinforcement exerted a significant influence on the ultimate load, failure was ruled by transverse bending. Once longitudinal failure was reached, a further increase of the amount of welded mesh did not produce an increment of the element bearing capacity, as demonstrated by the plateau of the curves of Figure 14a. From the first point of the plateau onwards, failure was governed indeed by the yielding of prestressing strands and transverse collapse was postponed with respect to the longitudinal one. In order to underline this aspect, a circle was drawn on the graphs of Figure 14a when the numerical analyses showed a transverse failure of the element; otherwise, a longitudinal "beam-like" failure was recorded. This is well highlighted in the chart of Figure 14a for the design cases C and D: the "limit" amount of transverse reinforcement corresponding to the transition from transverse to longitudinal failure was represented by Φ8/150 for a value of η_0 almost equal to 1.2. The minimum investigated amount of transverse reinforcement (i.e. Φ6/200) was associated to a coefficient η_0 slightly greater than 1, even if a transverse failure took place. It can be observed that the increase of the numerical resistance with respect to the design sectional one is more evident in the case of longitudinal failure, since the unfavourable effects related to geometric non-linearity are counterbalanced by the increased transverse reinforcement.

The same chart also points out that for a given transverse reinforcement percentage ρ, coefficient η_0 decreases with the increasing of complementary element dead load and with the increasing of spacing between roof elements. This corresponds to a progressively increasing reaction force at the top of each wing from case D (light panels, spacing 4.5 m) to case A (heavy panels, spacing 5.5 m), which in turn led to higher transverse stresses in the wings themselves. For a given configuration (A, B, C, D), the reduction of transverse reinforcement, whose main function is to bear transverse stresses, caused a corresponding decrease of coefficient η_0.

In order to better understand the influence of the amount of transverse reinforcement on the global behavior of the thin-walled element, numerical results were also reported in Figure 14b in terms of acting bending moment M vs. midspan deflection δ, for the design case A. As long as the failure was ruled by transverse stresses, an increase of welded mesh not only led to a higher ultimate resistance, but also to a greater ductility.

The influence of transverse reinforcement on failure mode can be appreciated also from the contours at failure concerning crack pattern, longitudinal stress in the strands and transverse strain of welded meshes. These were reported in Figures 15 and 16 for design case A, with reference to the minimum and maximum transverse reinforcement percentage (i.e. Φ6/200 and Φ10/120 mm), respectively. When the minimum transverse reinforcement amount was adopted, numerical analyses showed a transverse failure: the "critical" FE elements were placed at about mid-height of the wing, where transverse strains were higher (i.e. greater than a conventional value, here assumed equal to 10‰, Fig. 15a), while strands were still far from their limit design value (Fig. 15b). At failure, numerical crack pattern at extrados showed an extended longitudinal crack at mid-height of the wing (Fig. 15c), characterized by noticeable values of crack opening w. This crack appeared also at intrados near supports (Fig. 15d). On the contrary, when maximum transverse reinforcement was used, crack pattern at extrados (Fig. 16c) was characterized by more widespread cracks (also of flexural type), with lower width. Meanwhile, at element intrados, flexural cracks clearly appeared at midspan (Fig.16d), reaching significant a width at failure. Longitudinal failure was also confirmed by the yielding of strands (Fig. 16b), while strains in transverse reinforcement did not reach the 10‰ value (Fig. 16a).

5 Conclusions

The paper discusses the main results of an experimental and numerical investigation on a precast roof element with open cross section. The research work was organized in three main steps:

1) execution of a full-scale experimental test on a long span specimen, according to Product Standard EN 13693:2009;

2) validation of the adopted numerical procedure, taking into account both material non-linearity (by means of 2D-PARC model for RC elements) and second order effects, through comparisons with experimental results;

3) application of the abovementioned numerical procedure to a parametric study for the assessment of the influence exerted by the amount of transverse reinforcement on the expected failure mode. The main results of this study were summarized in the form of an "optimization design chart", relating the amount of transverse reinforcement to a coefficient of "model inaccuracy" η_0, to be applied for correcting simplified beam-like design calculations. Based on the obtained results, the following observations can be drawn:

– if $\eta_0 < 1$, element behavior is strongly influenced by second order effects and transverse failure occurs before the longitudinal one. For this reason, routine calculations based on beam theory should be adjusted by multiplying the design moment resistance M_{Rd} for η_0;

– if $\eta_0 \geq 1$, element design carried out according to beam theory can be considered safe since the actual bearing capacity of the element is greater than the design resistance obtained from routine calculations. However, this condition alone does not ensure that transverse failure is prevented, since element over-strength may be simply related to all the resistant mechanisms that develop after cracking;

– the failure mode can be correctly identified from the trend of the curves plotted in the "optimization design chart". When the failure is ruled by second order effects, coefficient η_0 increases with growing amounts of transverse reinforcement, while when longitudinal failure takes place, η_0 remains constant independently from any transverse reinforcement variation, and the curves show a plateau. From the first point of the plateau onwards, failure is governed by the yielding of prestressing strands and the behavior of the element follows classic beam theory.

Acknowledgments

Authors gratefully acknowledge EDILESSE S.r.l. (Reggio Emilia, Italy) for funding the research work and allowing the publication of the results.

References

[1] J.F. Doyle, Nonlinear analysis of thin-walled structures: statics, dynamics, and stability, Springer Science & Business Media, 2001.

[2] J.P. Papangelis, G.J. Hancock, Computer analysis of thin-walled structural members, Comput. Struct. 56 (1995) 157–176.

[3] Y. Pi, M.A. Bradford, Effects of approximations in analyses of beams of open thin-walled cross-section—part I: Flexural–torsional stability, Int. J. Numer. Methods Eng. 51 (2001) 757–772.

[4] X. Wang, Q. Yang, Geometrically nonlinear finite element model of spatial thin-walled beams with general open cross section, Acta Mech. Solida Sin. 22 (2009) 64–72.

[5] W. Derkowski, Large panels buildings–the possibilities of modern precast industry, Cem. Wapno Bet. 2017 (2017) 414–425.

[6] EN 13693:2009. Precast concrete products - Special roof elements, European Standard, 2009.

[7] EN 1992-1-1:2015, Eurocode 2 - Design of concrete structures - Part 1-1 : General rules and rules for buildings, 2015.

[8] S. Carbonari, F. Gara, D. Roia, G. Leoni, L. Dezi, Tests on two 18-years-old prestressed thin walled roof elements, Eng. Struct. 49 (2013) 936–946.

[9] B. Belletti, P. Bernardi, E. Michelini, Behavior of thin-walled prestressed concrete roof elements - Experimental investigation and numerical modeling, Eng. Struct. 107 (2016) 166–179. doi:10.1016/j.engstruct.2015.06.058.

[10] B. Dal Lago, Experimental and numerical assessment of the service behaviour of an innovative long-span precast roof element, Int. J. Concr. Struct. Mater. 11 (2017) 261–273.

[11] B. Belletti, Evaluation of the interaction effects in coupled thin walled prestressed concrete roof elements, Eur. J. Environ. Civ. Eng. 13 (2009) 745–764.

[12] M. di Prisco, D. Dozio, B. Belletti, On the fracture behaviour of thin-walled SFRC roof elements, Mater. Struct. 46 (2013) 803–829.

[13] A. Bergamini, F. Biondini, Finite strip modeling for optimal design of prestressed folded plate structures, Eng. Struct. 26 (2004) 1043–1054.

[14] B. Balogh, J. Lógó, Optimal design of curved folded plates, Period. Polytech. Civ. Eng. 58 (2014) 423–430.

[15] V. Albero, A. Espinós, E. Serra, M.L. Romero, A. Hospitaler, Numerical study on the flexural behaviour of slim-floor beams with hollow core slabs at elevated temperature, Eng. Struct. 180 (2019) 561–573.

[16] ABAQUS Analysis User's Manual, Dassault Systèmes Simulia Corp., Providence, RI, USA, n.d.

[17] R. Cerioni, I. Iori, E. Michelini, P. Bernardi, Multi-directional modeling of crack pattern in 2D R/C members, Eng. Fract. Mech. 75 (2008) 615–628. doi:10.1016/j.engfracmech.2007.04.012.

[18] P. Bernardi, R. Cerioni, E. Michelini, A. Sirico, Numerical modeling of the cracking behavior of RC and SFRC shear-critical beams, Eng. Fract. Mech. 167 (2016) 151–166. doi:10.1016/j.engfracmech.2016.04.008.

[19] K. Flaga, W. Derkowski, M. Surma, Concrete strength and elasticity of precast thin-walled elements, Cem. Wapno Bet. 21/83 (2016) 310–317.

List of Figures

Figure 1 – Investigated three-plate roof element: (a) application in an industrial building; (b) sketch of the current cross section (dimensions in mm) with reinforcement arrangement of the tested specimen.

Figure 2 – (a) General view of test setup; detail of support condition: (b) lateral view, (c) top view.

Figure 3 – Sketch of the loading arrangement: (a) lateral view; (b) top and transverse views; (c), (d) detail of the load application system in the transverse cross section.

Figure 4 – (a) Sketch of the position of the adopted instrumentation for the measurement of (b) vertical and horizontal displacements in sections D-W, (c) longitudinal strains in section L-S, (d) transverse strains in section T-S.

Figure 5 – View of the adopted instrumentation: (a) strain gauge on the element extrados; (b), (c) transducers for displacement acquisition.

Figure 6 –Total load on the roof element (P) vs. (a) vertical displacement in the bottom chord (δ_c) in the three loaded sections; (b) transverse strain at wing extrados and at bottom chord intrados.

Figure 7 – Evolution of the experimental crack pattern: (a) vertical flexural cracks at midspan; (b) inclined flexural-shear cracks between midspan and the support; (c) crack near the support at element extrados; (d) inclined shear cracks at the support; (e) longitudinal cracks at mid-height of wing extrados; (f) loss of shape of the open cross section in its own plane.

Figure 8 – Calibration of support stiffness on the basis of the experimental measurements, in terms of reaction forces (RF) vs. vertical displacement of the bottom chord (δ_c) at supports.

Figure 9 – Comparisons between numerical and experimental results in terms of total load (P) vs. vertical displacement at the bottom chord (δ_c) and on the top of the wings (δ_w) in the loaded sections: (a), (b) at midspan; (c), (d) at one-sixth of the span.

Figure 10– Comparisons between numerical and experimental results in terms of total load (P) vs. horizontal displacement of the wing (u_w): (a) at one-sixth of the span and (b) at supports.

Figure 11 – Comparisons between numerical and experimental results at element extrados (a-d) and intrados (e-f) in terms of total load (P) vs. longitudinal strain on the wings (a) and at the bottom chord (b) and vs. transverse strain on the wings (c, e) and at the bottom chord (d, f).

Figure 12 – Comparisons between numerical and experimental results in terms of crack pattern at failure at element intrados: (a) at midspan and (b) near supports.

Figure 13 – Comparisons between numerical and experimental results in terms of crack pattern at failure at element extrados.

Figure 14 – (a) optimization chart for the four cases examined (A, B, C, D) in terms of ratio η_0 between numerical and theoretical flexural bearing capacity vs. transverse reinforcement percentage ρ, (b) numerical results in terms of bending moment M vs. midspan deflection δ for case A, for different transverse reinforcement percentage.

Figure 15 – NLFEA results at failure for design case A with transverse reinforcement Φ6/200 mm: (a) transverse strain in the steel welded mesh; (b) stress in prestressing strands; (c), (d) crack pattern and corresponding crack opening w at element extrados and intrados, respectively.

Figure 16 – NLFEA results at failure for design case A with transverse reinforcement Φ10/120 mm: (a) transverse strain in the steel welded mesh; (b) stress in prestressing strands; (c), (d) crack pattern and corresponding crack opening w at element extrados and intrados, respectively.

List of Tables

Table 1 – Concrete and steel mean mechanical properties.

Table 2 – Experimental loading sequence.

Table 3 – Definition of the reference cases for NLFE design optimization analyses.

(a)

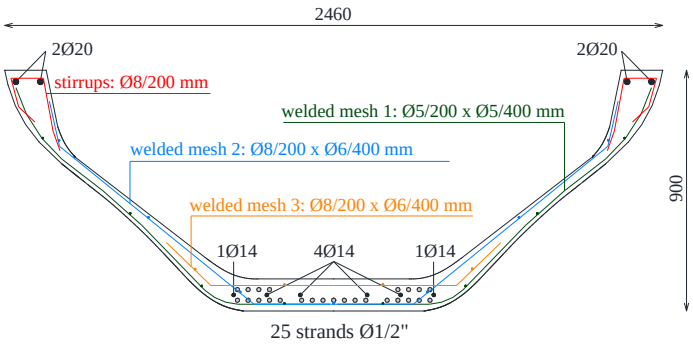

(b)

Figure 1 – Investigated three-plate roof element: (a) application in an industrial building; (b) sketch of the current cross section (dimensions in mm) with reinforcement arrangement of the tested specimen.

(a)

(b)

(c)

Figure 2 – (a) General view of test setup; detail of support condition: (b) lateral view, (c) top view.

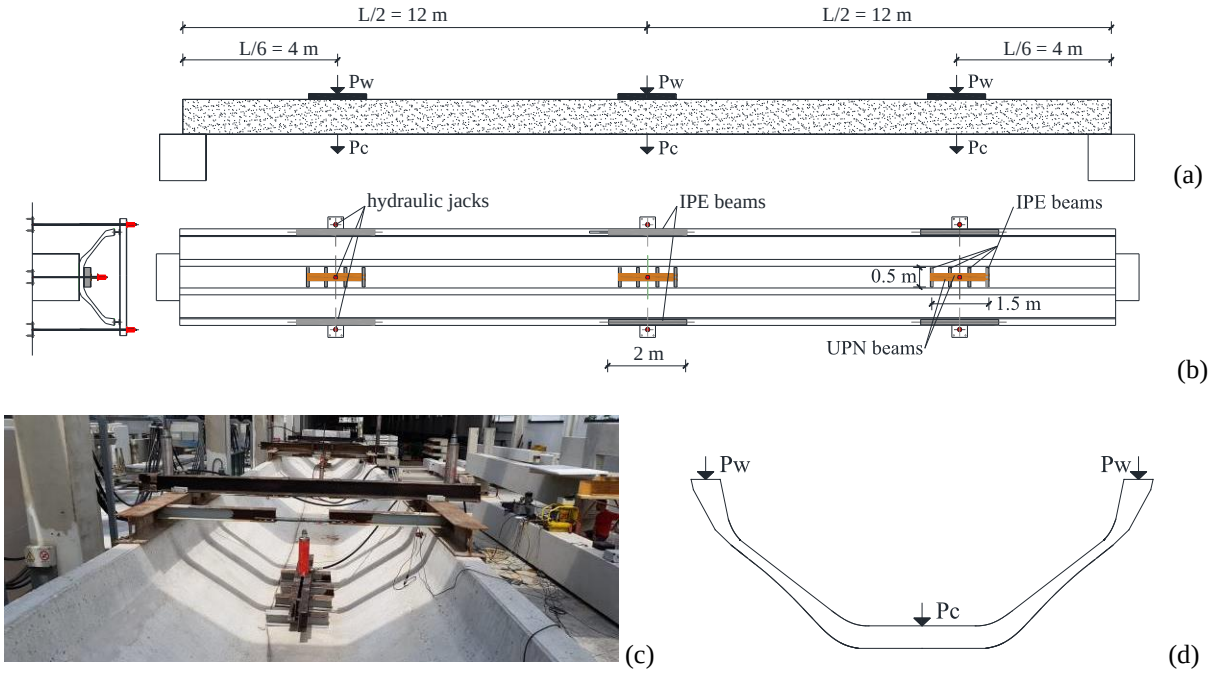

Figure 3 – Sketch of the loading arrangement: (a) lateral view; (b) top and transverse views; (c), (d) detail of the load application system in the transverse cross section.

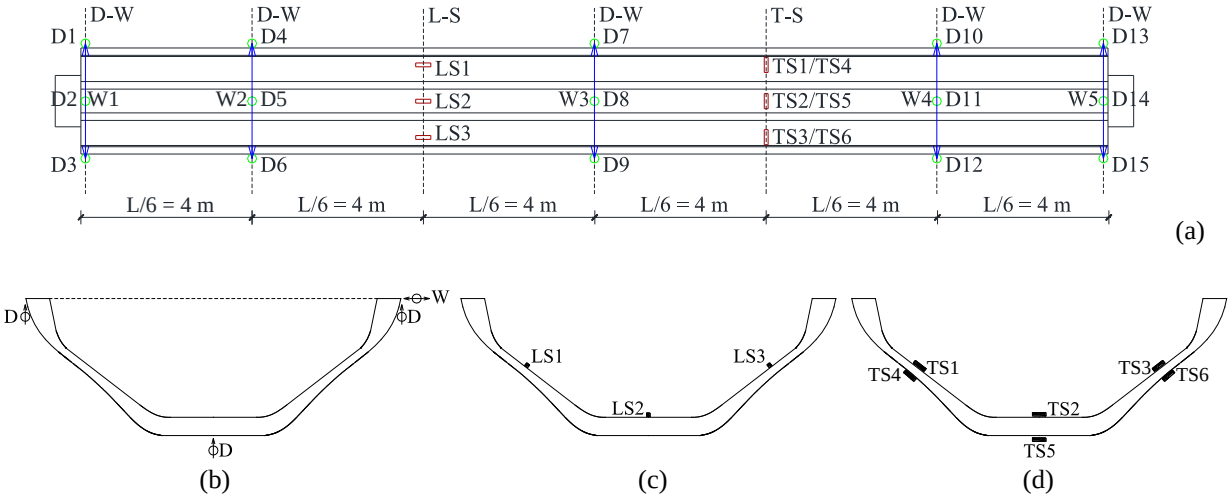

Figure 4 – (a) Sketch of the position of the adopted instrumentation for the measurement of (b) vertical and horizontal displacements in sections D-W, (c) longitudinal strains in section L-S, (d) transverse strains in section T-S.


(a)

(b)

(c)

Figure 5 – View of the adopted instrumentation: (a) strain gauge on the element extrados; (b), (c) transducers for displacement acquisition.

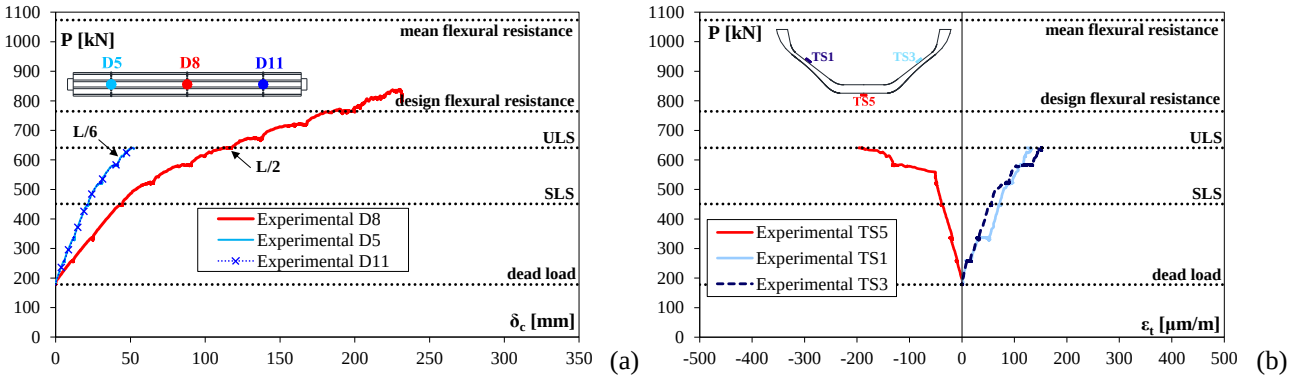

Figure 6 –Total load on the roof element (P) vs. (a) vertical displacement in the bottom chord (δ_c) in the three loaded sections; (b) transverse strain at wing extrados and at bottom chord intrados.

Figure 7 – Evolution of the experimental crack pattern: (a) vertical flexural cracks at midspan; (b) inclined flexural-shear cracks between midspan and the support; (c) crack near the support at element extrados; (d) inclined shear cracks at the support; (e) longitudinal cracks at mid-height of wing extrados; (f) loss of shape of the open cross section in its own plane.

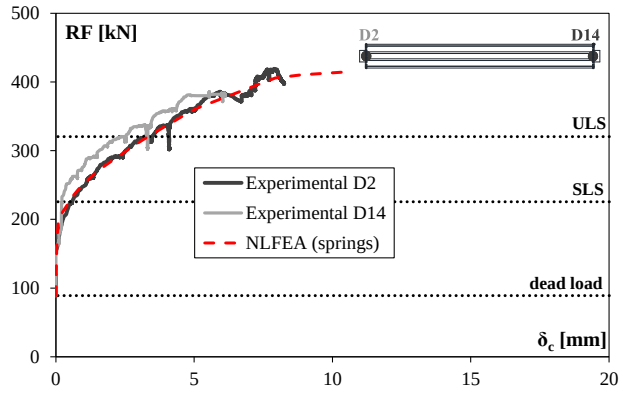

Figure 8 – Calibration of support stiffness on the basis of the experimental measurements, in terms of reaction forces (RF) vs. vertical displacement of the bottom chord (δ_c) at supports.

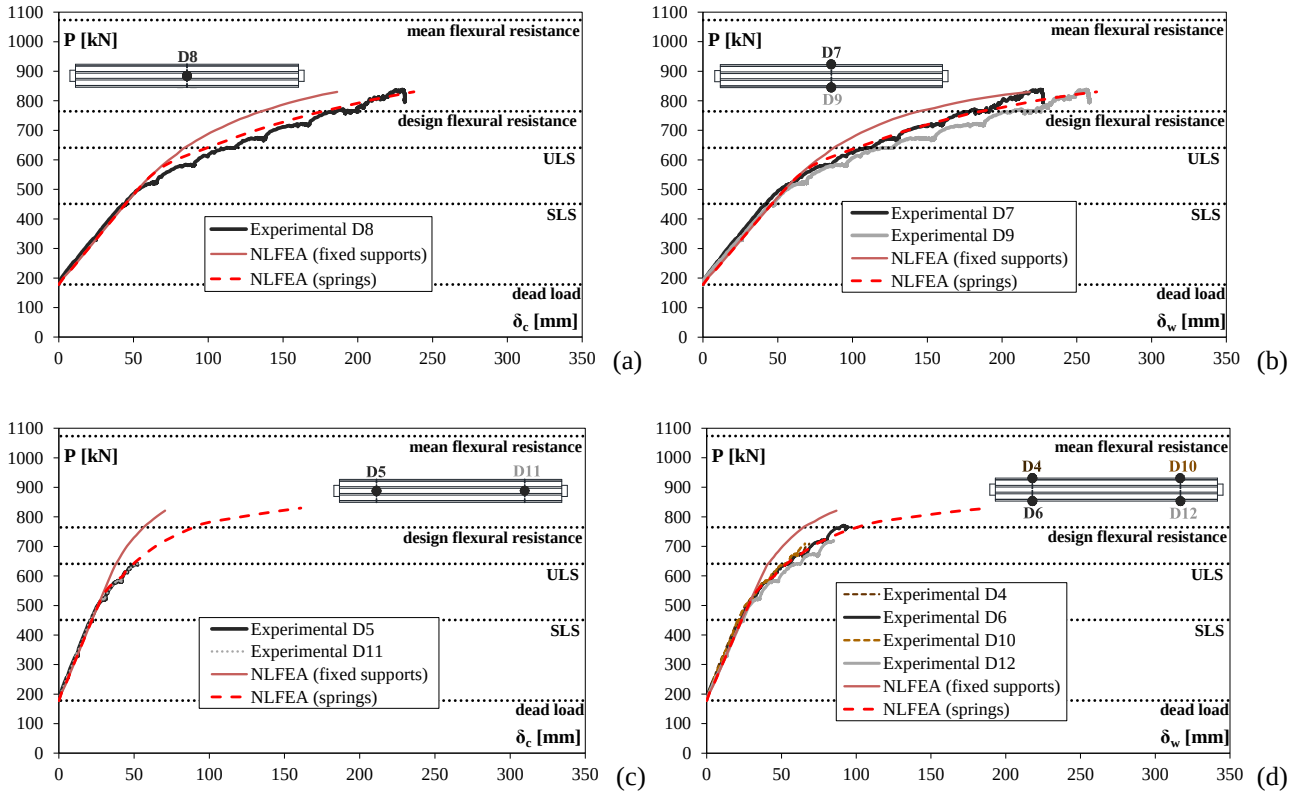

Figure 9 – Comparisons between numerical and experimental results in terms of total load (P) vs. vertical displacement at the bottom chord (δ_c) and on the top of the wings (δ_w) in the loaded sections: (a), (b) at midspan; (c), (d) at one-sixth of the span.

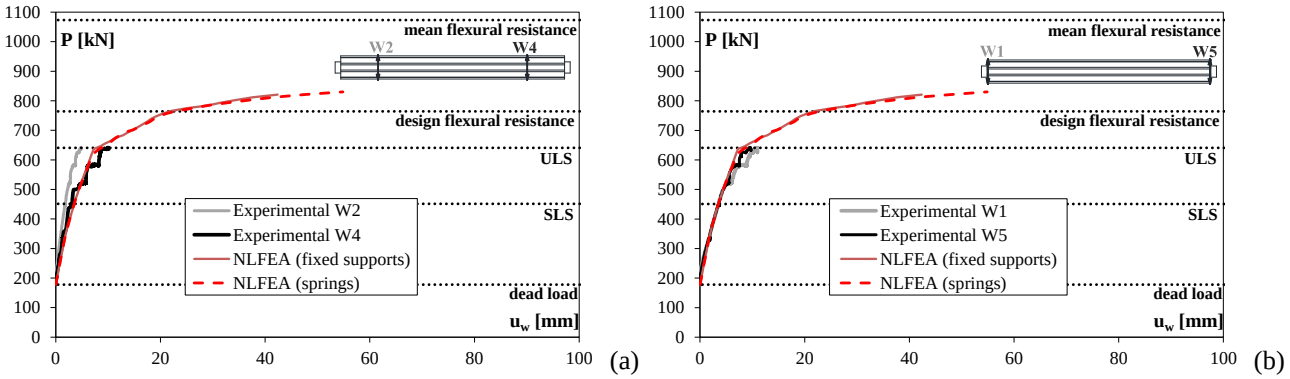

Figure 10– Comparisons between numerical and experimental results in terms of total load (P) vs. horizontal displacement of the wing (u_w): (a) at one-sixth of the span and (b) at supports.

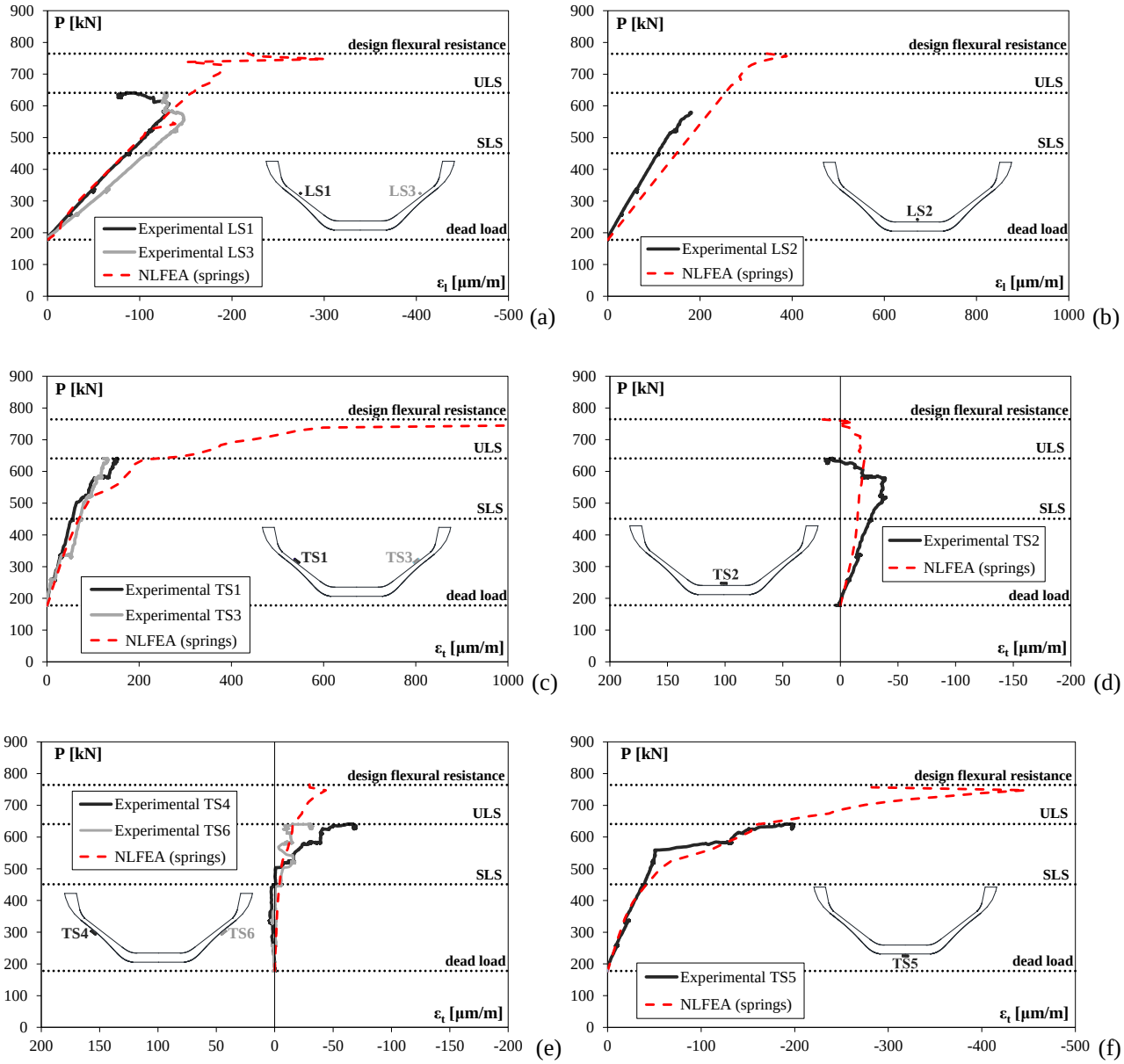

Figure 11 – Comparisons between numerical and experimental results at element extrados (a-d) and intrados (e-f) in terms of total load (P) vs. longitudinal strain on the wings (a) and at the bottom chord (b) and vs. transverse strain on the wings (c, e) and at the bottom chord (d, f).

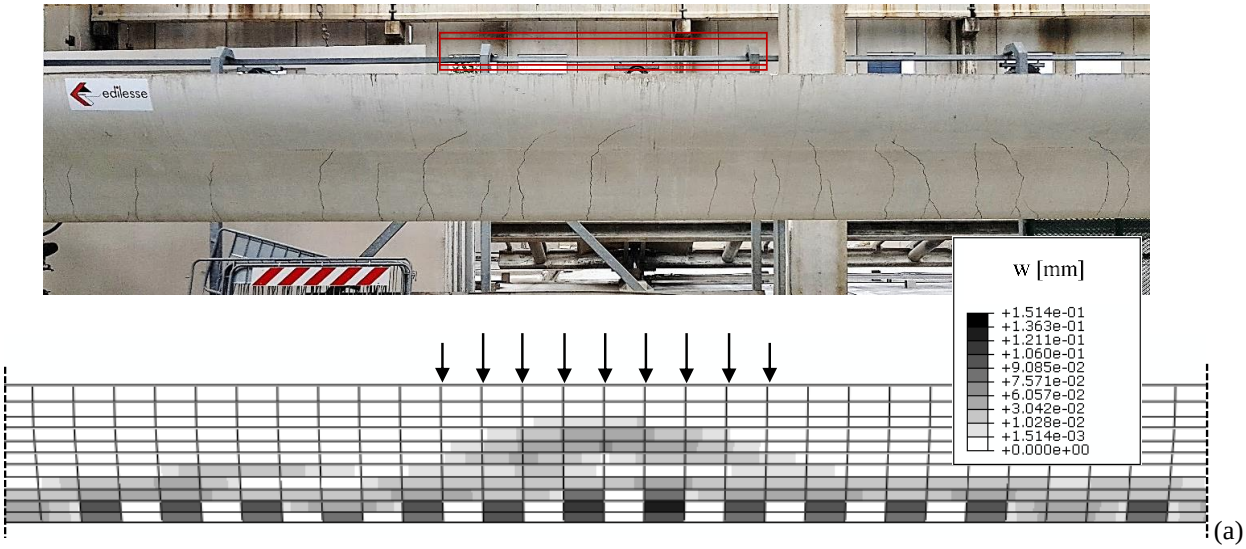

(a)

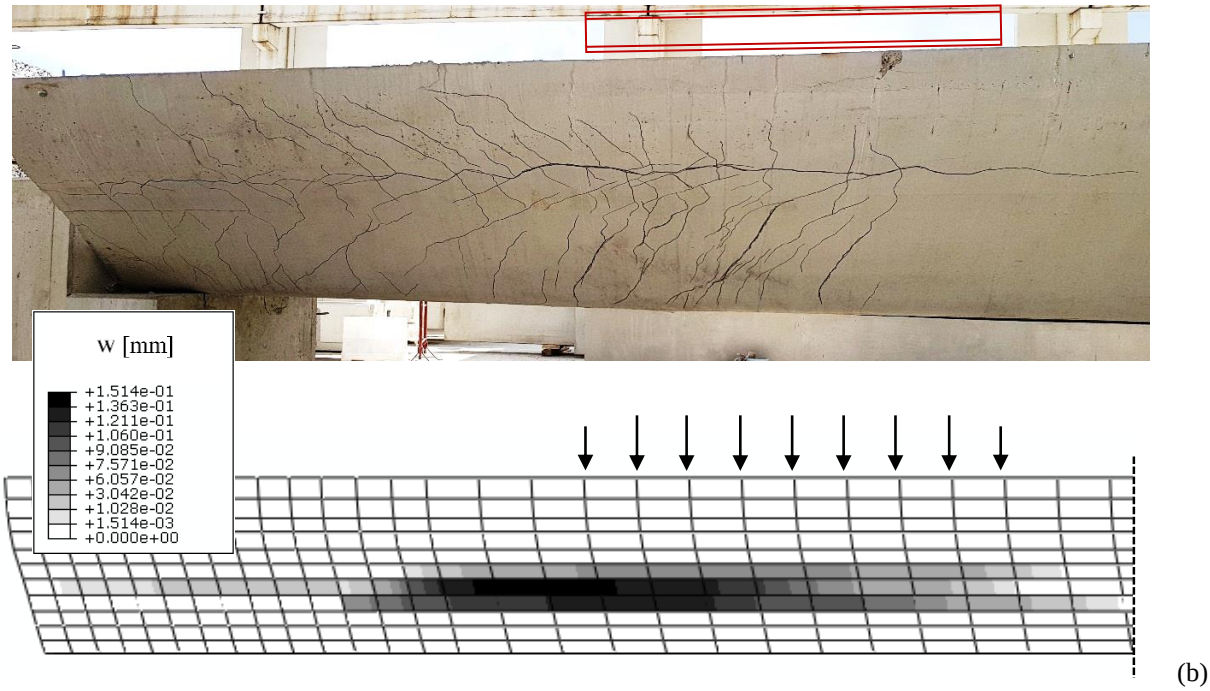

(b)

Figure 12 – Comparisons between numerical and experimental results in terms of crack pattern at failure at element intrados: (a) at midspan and (b) near supports.

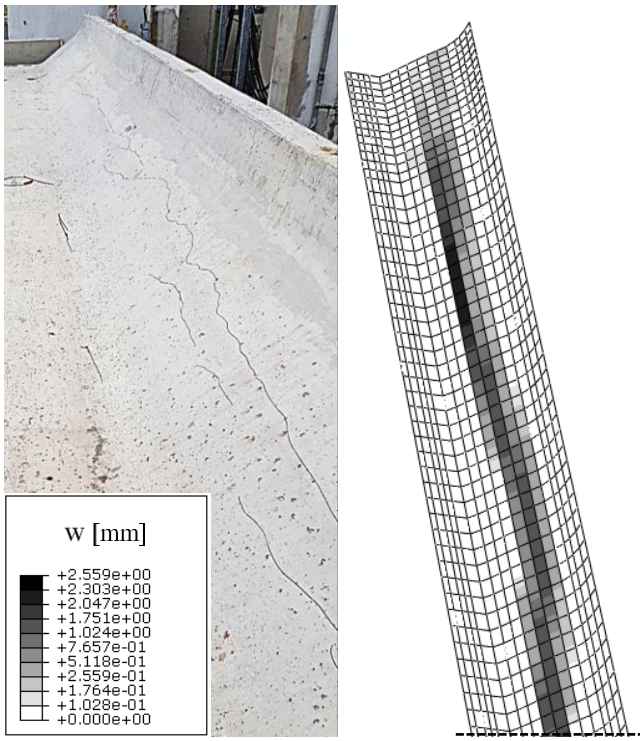

Figure 13 – Comparisons between numerical and experimental results in terms of crack pattern at failure at element extrados.

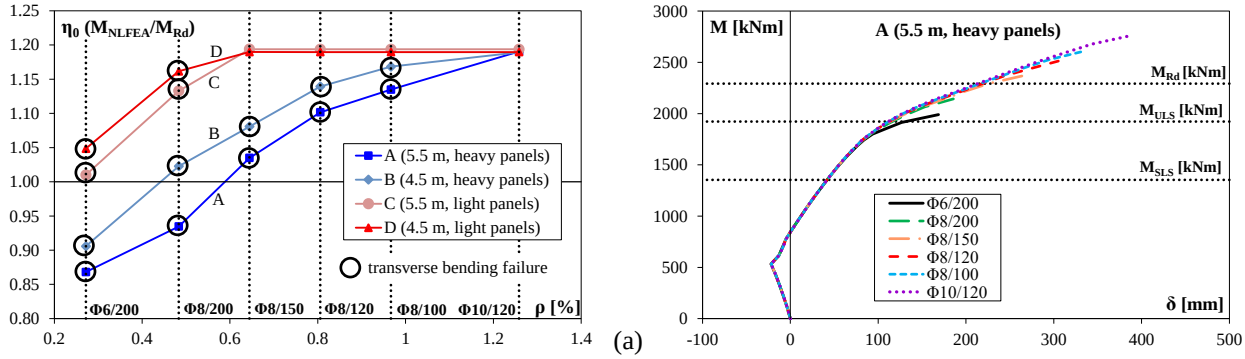

Figure 14 – (a) optimization chart for the four cases examined (A, B, C, D) in terms of ratio η_0 between numerical and theoretical flexural bearing capacity vs. transverse reinforcement percentage ρ, (b) numerical results in terms of bending moment M vs. midspan deflection δ for case A, for different transverse reinforcement percentage.

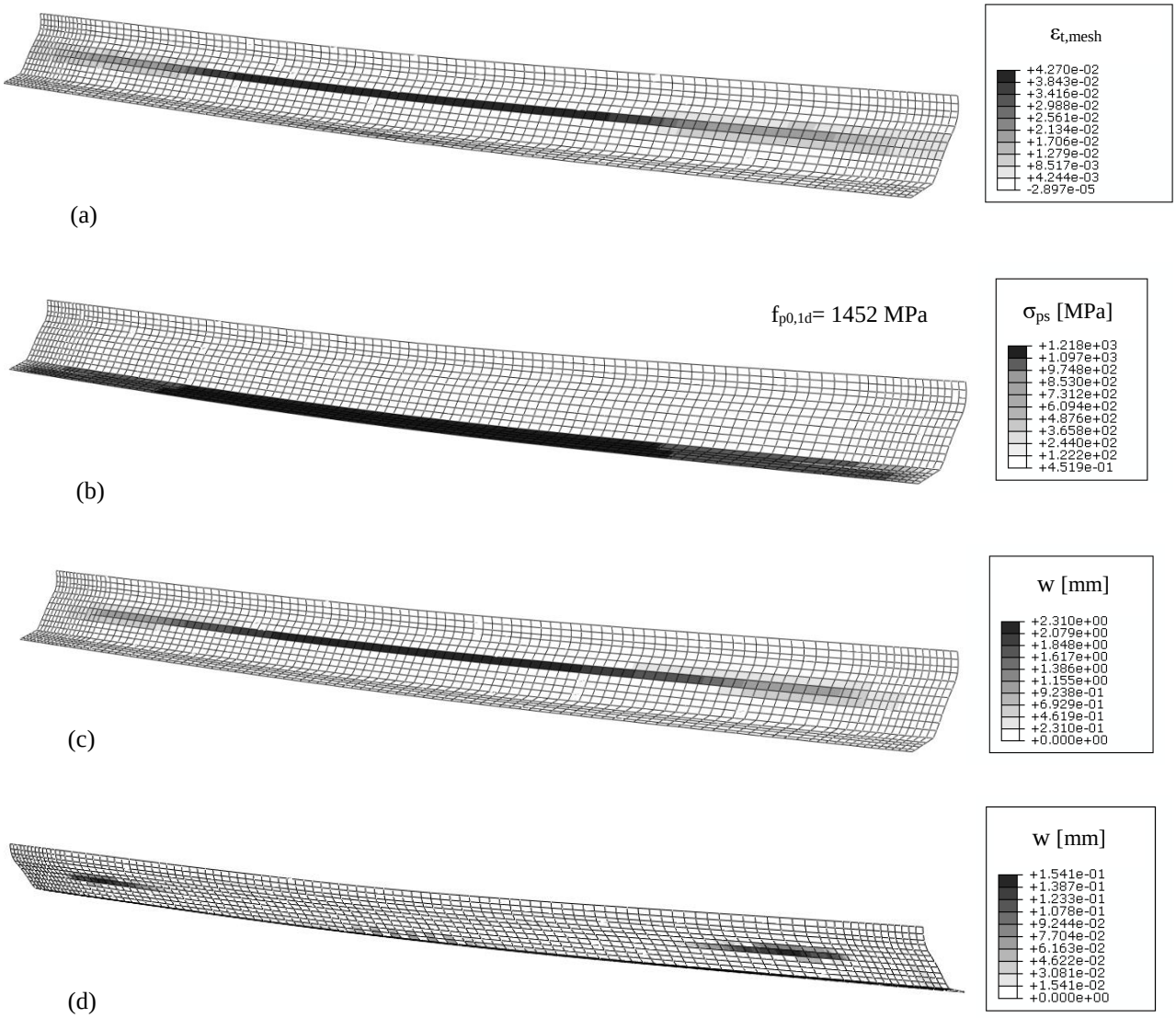

Figure 15 – NLFEA results at failure for design case A with transverse reinforcement Φ6/200 mm: (a) transverse strain in the steel welded mesh; (b) stress in prestressing strands; (c), (d) crack pattern and corresponding crack opening w at element extrados and intrados, respectively.

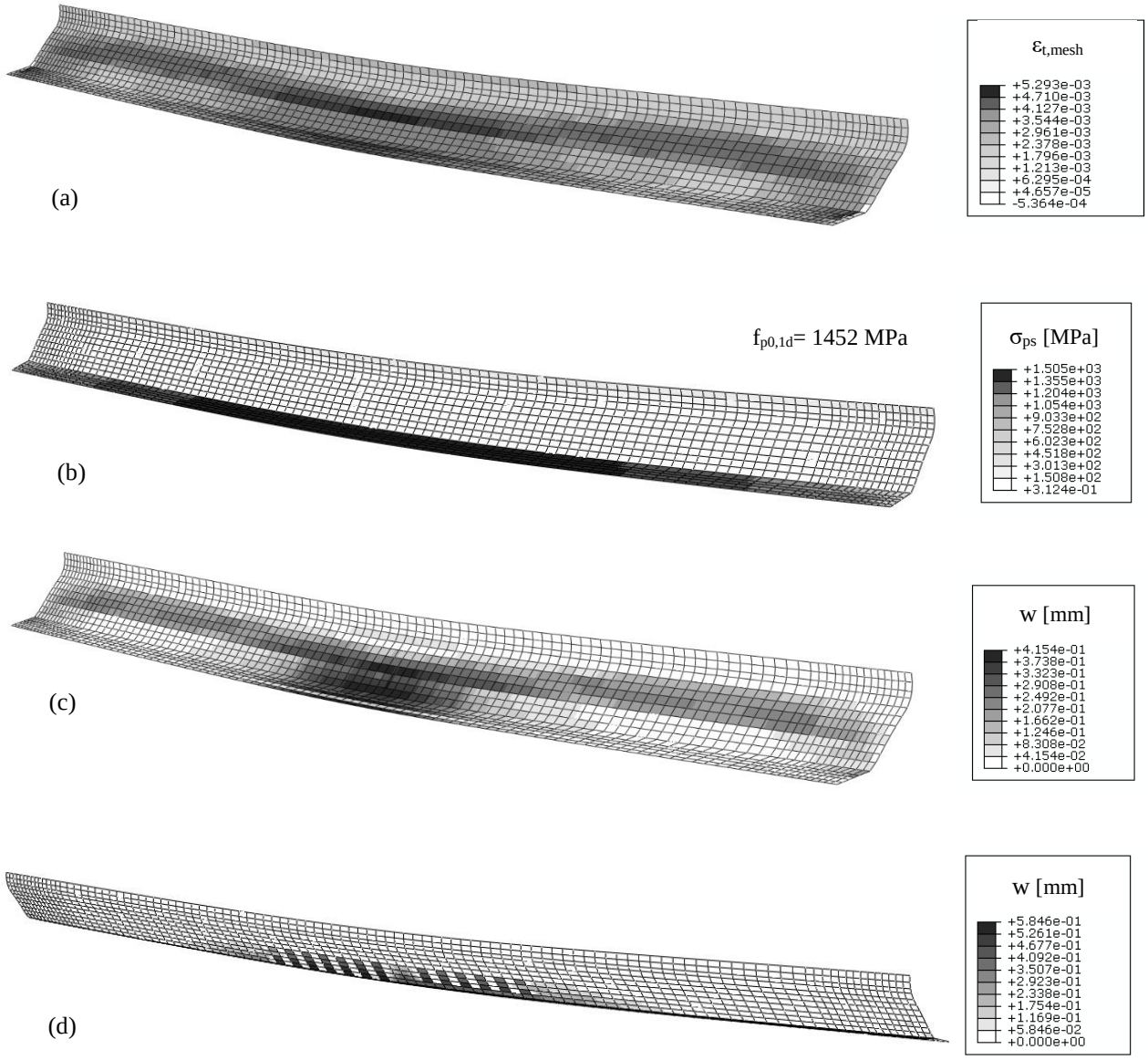

Figure 16 – NLFEA results at failure for design case A with transverse reinforcement Φ10/120 mm: (a) transverse strain in the steel welded mesh; (b) stress in prestressing strands; (c), (d) crack pattern and corresponding crack opening w at element extrados and intrados, respectively.

Concrete	$f_{c,cube}$*(MPa) *65*			
Ordinary steel	f_y (MPa) 486	f_t (MPa) 583		
Prestressing steel	$f_{p0,1}$ (MPa) 1712	$f_{p(1)}$ (MPa) 1730	$f_{p,}$ (MPa) 1930	E_p (MPa) 202238

* at the day of testing

Table 1 – Concrete and steel mean mechanical properties.

	Loading steps	P_c [kN] (bottom chord)	P_w [kN] (wings)
Loading Cycle n°1	1	5.00	2x10.75
	2	10.00	2x21.50
	3 (SLS)	17.00	2x36.55
	2	10.00	2x21.50
	1	5.00	2x10.75
	Loading steps	**P_c [kN] (bottom chord)**	**P_w [kN] (wings)**
Loading Cycle n°2	1	5.00	2x10.75
	2	10.00	2x21.50
	3 (SLS)	17.00	2x36.55
	2	10.00	2x21.50
	1	5.00	2x10.75
	Loading steps	**P_c [kN] (bottom chord)**	**P_w [kN] (wings)**
Loading Cycle n°3	1	5.00	2x10.75
	2	10.00	2x21.50
	3 (SLS)	17.00	2x36.55
	4	23.50	2x45.80
	5	30.00	2x52.50
	6 (ULS)*	37.00	2x58.00
	7	40.00	2x62.50
	8	43.75	2x68.40
	9 (M_{Rd})	47.50	2x74.25
	10	49.25	2x77.00
	11	51.20	2x80.00
	12	53.20	2x83.00

*partial removal of the applied instrumentation

Table 2 – Experimental loading sequence.

Case	Spacing [m]	Type of complementary element	Number of prestressing strands [ϕ = 1/2"]	Design moment resistance M_{Rd} [kNm]
A	5.5	heavy	25	2293
B	4.5	heavy	22	2229
C	5.5	light	18	2006
D	4.5	light	17	1939

Table 3 – Definition of the reference cases for NLFE design optimization analyses.